Quantum Monte Carlo calculations of neutron matter with chiral three-body forces

I. Tews, S. Gandolfi, A. Gezerlis, and A. Schwenk

Phys. Rev. C **93**, 024305 — Published 2 February 2016

DOI: 10.1103/PhysRevC.93.024305

Quantum Monte Carlo calculations of neutron matter with chiral three-body forces

I. Tews,[1,2,*] S. Gandolfi,[3,†] A. Gezerlis,[4,‡] and A. Schwenk[1,2,§]

[1] *Institut für Kernphysik, Technische Universität Darmstadt, 64289 Darmstadt, Germany*
[2] *ExtreMe Matter Institute EMMI, GSI Helmholtzzentrum für Schwerionenforschung GmbH, 64291 Darmstadt, Germany*
[3] *Theoretical Division, Los Alamos National Laboratory, Los Alamos, NM 87545, USA*
[4] *Department of Physics, University of Guelph, Guelph, Ontario N1G 2W1, Canada*

Chiral effective field theory (EFT) enables a systematic description of low-energy hadronic interactions with controlled theoretical uncertainties. For strongly interacting systems, quantum Monte Carlo (QMC) methods provide some of the most accurate solutions, but they require as input local potentials. We have recently constructed local chiral nucleon-nucleon (NN) interactions up to next-to-next-to-leading order (N^2LO). Chiral EFT naturally predicts consistent many-body forces. In this paper, we consider the leading chiral three-nucleon (3N) interactions in local form. These are included in auxiliary field diffusion Monte Carlo (AFDMC) simulations. We present results for the equation of state of neutron matter and for the energies and radii of neutron drops. In particular, we study the regulator dependence at the Hartree-Fock level and in AFDMC and find that present local regulators lead to less repulsion from 3N forces compared to the usual nonlocal regulators.

PACS numbers: 21.60.Ka, 21.30.x, 21.65.Cd, 26.60.c

I. INTRODUCTION

Chiral EFT provides a systematic expansion for nuclear forces based on the symmetries of QCD [1–3]. At a given order in the power counting, nuclear forces include contributions from pion exchanges and from shorter-range interactions. Chiral EFT enables calculations with controlled theoretical uncertainties, a consistent description of electroweak interactions, and the matching to lattice QCD. In addition to NN interactions, which are the dominant contribution to nuclear forces, chiral EFT naturally predicts consistent many-body interactions, where the leading 3N forces enter at N^2LO [4, 5]. It has been shown that 3N forces are key for the properties of neutron and nuclear matter [6–14]. A better understanding of 3N forces is a major frontier in nuclear physics.

In addition to systematic chiral EFT interactions, reliable many-body methods are needed. For strongly interacting systems, QMC methods provide some of the most accurate solutions [15, 16]. These include Green's function Monte Carlo (GFMC) [17–19] and AFDMC [20] methods, for a recent review see Ref. [21]. In continuum QMC calculations, the central object is the many-body propagator, which is of the form

$$G(\mathbf{R}, \mathbf{R}'; \delta\tau) = \langle \mathbf{R} | e^{-\delta\tau \widehat{H}} | \mathbf{R}' \rangle \,. \tag{1}$$

Here, $\mathbf{R} = (\mathbf{r}_1, s_1, \mathbf{r}_2, s_2, \ldots, \mathbf{r}_N, s_N)$ is the configuration vector of all N particles, including the single-particle coordinates and spins $\mathbf{r}_i, s_i$ (and other quantum numbers), $\delta\tau$ is a step in the imaginary-time evolution, and $\widehat{H}$ is the Hamiltonian.

In nuclear GFMC calculations all possible spin-isospin nucleon states need to be explicitly accounted for, which makes this method unsuitable for accurate neutron matter studies due to an unfavorable scaling behavior. In contrast to GFMC, AFDMC rewrites the Green's function by applying a Hubbard-Stratonovich transformation using auxiliary fields, which changes the scaling behavior favorably at the cost of additional integrations over auxiliary fields. We thus make use of the AFDMC method to study neutron matter.

The trial wave function ψ_T in AFDMC is usually chosen to be of the form

$$\psi_T(\mathbf{R}) = \left[\prod_{i<j} f_J(r_{ij}) \right] \Phi_A(\mathbf{R}) \,, \tag{2}$$

where inter-particle correlations are included through the Jastrow factor $f_J(r_{ij})$ and Φ_A is the noninteracting ground state given by a Slater determinant

$$\Phi_A(\mathbf{R}) = \mathcal{A} \left[\prod_i \phi_{\alpha_i}(\mathbf{r}_i, s_i) \right] \,, \tag{3}$$

where α_i labels single-particle states (plane waves for neutron matter and Hartree-Fock orbitals for neutron drops [22]).

For the evaluation of the propagator, it is necessary to be able to separate all momentum dependences as a quadratic $\sum_{i=1}^{N} \mathbf{p}_i^2$ term. This can be done for local interactions, where the propagator for the momentum-dependent part is a Gaussian integral that can be evaluated analytically, while the interaction part can be easily obtained from the configuration vector (for more details see Ref. [21]). Chiral EFT interactions are naturally formulated in momentum space and usually contain several sources of nonlocality.

Recently, local chiral NN potentials have been constructed up to N^2LO and have been used to calculate

* E-mail: tews@theorie.ikp.physik.tu-darmstadt.de
† E-mail: stefano@lanl.gov
‡ E-mail: gezerlis@uoguelph.ca
§ E-mail: schwenk@physik.tu-darmstadt.de

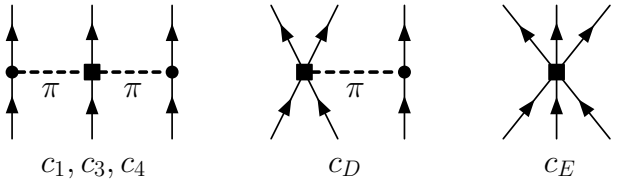

FIG. 1. Contributions to 3N forces at N^{2}LO. These include a two-pion-exchange part given by the couplings c_1, c_3, and c_4, a one-pion-exchange–contact interaction given by c_D, and a 3N contact interaction given by c_E.

the energy of neutron matter and light nuclei using continuum QMC methods [23–25]. Following the same strategy, a minimally nonlocal NN potential was developed in Ref. [26] with explicit Δ degrees of freedom. Monte Carlo methods have also been used to study neutron matter based on lattice techniques [27] and with momentum-space QMC approaches [28, 29].

For a complete calculation at N^{2}LO, it is necessary to include 3N forces. In Sec. II, we present local chiral 3N forces at N^{2}LO, which are consistent with the local NN interactions of Refs. [23, 24]. The general expressions for the local 3N forces are given in Appendix A. We study in detail the regulator dependence of the leading two-pion-exchange 3N energy contributions at the Hartree-Fock level in Sec. III and in AFDMC in Sec. IV. This shows that present local regulators lead to less repulsion from 3N forces compared to using the usual nonlocal regulators. We present results for the equation of state of neutron matter in Sec. IV and for the energies and radii of neutron drops in Sec. V. Finally, we summarize and give an outlook.

II. CHIRAL 3N FORCES IN COORDINATE SPACE

In chiral EFT, the leading 3N forces at N^{2}LO have three contributions: a two-pion-exchange part given by the couplings c_1, c_3, and c_4, a one-pion-exchange–contact interaction given by c_D, and a 3N contact interaction given by c_E [4, 5]. We show the N^{2}LO 3N contributions diagrammatically in Fig. 1. The c_i couplings are determined by pion-nucleon or NN scattering, while c_D and c_E have to be fit to properties of $A > 2$ systems.

Because we want to include 3N forces in AFDMC calculations in coordinate space, we have to use local coordinate-space expressions of the N^{2}LO 3N forces, as was similarly done in Refs. [30, 31]. To achieve this, we first Fourier transform the momentum-space expressions of the N^{2}LO 3N forces. We begin with the 3N contact interaction V_E. In momentum space, this contribution vanishes in neutron matter due to the Pauli principle, when a regulator that is symmetric in the particle labels is used, see Ref. [6]. Because a local regulator does not fulfill this requirement, the V_E term will contribute. In this case, the regulator induces a finite range that mixes 3N partial waves. After Fourier transformation, we find in neutron matter (with $\boldsymbol{\tau}_i \cdot \boldsymbol{\tau}_k = 1$)

$$V_E^{ijk} = \frac{c_E}{2 f_\pi^4 \Lambda_\chi} \sum_{\pi(ijk)} \delta(\mathbf{r}_{ij}) \delta(\mathbf{r}_{kj}) \,, \tag{4}$$

where we sum over all permutations $\pi(ijk)$ of the three particles i, j, and k, $\mathbf{r}_{ij} = \mathbf{r}_i - \mathbf{r}_j$, $f_\pi = 92.4\,\mathrm{MeV}$ is the pion decay constant, and we use $\Lambda_\chi = 700\,\mathrm{MeV}$. The expressions for general isospin and details on the Fourier transformation are provided in Appendix A.

As for the V_E term, the one-pion-exchange–contact interaction V_D vanishes in momentum space for neutron matter due to the spin-isospin structure, if a symmetric regulator is used [6]. In coordinate space, the V_D term also contributes and after Fourier transformation we have two parts (see Appendix A):

$$V_D^{ijk} = \frac{g_A}{24 f_\pi^4} \frac{c_D}{\Lambda_\chi} \sum_{\pi(ijk)} \Big[\frac{m_\pi^2}{4\pi} \delta(\mathbf{r}_{ij}) X_{ik}(\mathbf{r}_{kj}) - \boldsymbol{\sigma}_i \cdot \boldsymbol{\sigma}_k \, \delta(\mathbf{r}_{ij}) \delta(\mathbf{r}_{kj}) \Big] \,, \tag{5}$$

where $g_A = 1.267$ is the axial coupling, $m_\pi = 138.03\,\mathrm{MeV}$ is the averaged pion mass, and the function $X_{ik}(\mathbf{r})$ is given by

$$X_{ik}(\mathbf{r}) = \big[S_{ik}(\mathbf{r})\, T(r) + \boldsymbol{\sigma}_i \cdot \boldsymbol{\sigma}_k \big] Y(r) \,, \tag{6}$$

with the tensor operator $S_{ik}(\mathbf{r}) = 3\boldsymbol{\sigma}_i \cdot \hat{\mathbf{r}} \boldsymbol{\sigma}_k \cdot \hat{\mathbf{r}} - \boldsymbol{\sigma}_i \cdot \boldsymbol{\sigma}_k$, the function $T(r) = 1 + 3/(m_\pi r) + 3/(m_\pi r)^2$, and the Yukawa function $Y(r) = e^{-m_\pi r}/r$. Here, $\hat{\mathbf{r}}$ is the unit vector in the direction of $\mathbf{r}$ and r is the magnitude. There are two contributions from V_D, because one-pion exchange contains a long-range part as well as a delta-function part. The latter needs to be included to maintain the Goldstone boson nature of the pion.

We emphasize that there is an ambiguity in performing the Fourier transformation for the V_D term, depending on the choice of the initial spin-isospin structure. This leads either to terms $\delta(\mathbf{r}_{ij}) X_{ik}(\mathbf{r}_{kj})$ or $\delta(\mathbf{r}_{ij}) X_{kj}(\mathbf{r}_{kj})$ with different spin indices in the X function. The two expressions are the same due to the δ function, but lead to different results after regularization. Therefore, the differences from choosing different structures are a regulator effect and should be of higher order, as mentioned in Ref. [31]. These differences will vanish in the limit of infinite momentum cutoff. Because we will not include the V_D term in our calculations in this paper, this effect will not influence the results here. The different V_D terms will be studied in Ref. [32].

We now turn to the two-pion-exchange contributions V_C in neutron matter (see Appendix A). For the part proportional to c_1, we find

$$V_{C,c_1}^{ijk} = \frac{c_1 m_\pi^4 g_A^2}{2 f_\pi^4 (4\pi)^2} \sum_{\pi(ijk)} \boldsymbol{\sigma}_i \cdot \hat{\mathbf{r}}_{ij} \, \boldsymbol{\sigma}_k \cdot \hat{\mathbf{r}}_{kj} \times U(r_{ij}) Y(r_{ij}) U(r_{kj}) Y(r_{kj}) \,, \tag{7}$$

with the function $U(r) = 1 + 1/(m_\pi r)$. This contribution is similar to the long-range (LR) S-wave part of the Illinois 3N forces, see Ref. [33].

The part proportional to c_3 is given by

$$V_{C,c_3}^{ijk} = \frac{c_3 g_A^2}{36 f_\pi^4} \sum_{\pi(ijk)} \times \left[\frac{m_\pi^4}{(4\pi)^2} X_{ij}(\mathbf{r}_{ij}) X_{kj}(\mathbf{r}_{kj}) - \frac{m_\pi^2}{4\pi} X_{ik}(\mathbf{r}_{ij}) \delta(\mathbf{r}_{kj}) - \frac{m_\pi^2}{4\pi} X_{ik}(\mathbf{r}_{kj}) \delta(\mathbf{r}_{ij}) + \boldsymbol{\sigma}_i \cdot \boldsymbol{\sigma}_k \delta(\mathbf{r}_{ij})\, \delta(\mathbf{r}_{kj}) \right] . \quad (8)$$

Thus, in coordinate space, for the c_3 part of the V_C term, there are four contributions due to a long-range and short-range part in each pion exchange. The first term $\sim X_{ij}(\mathbf{r}_{ij}) X_{kj}(\mathbf{r}_{kj})$ is a long-range two-pion-exchange contribution similar to the anticommutator part of the P-wave two-pion-exchange interaction of Ref. [33]. In addition, there is also a short-range (SR) term $\sim \delta(\mathbf{r}_{ij})\delta(\mathbf{r}_{kj})$ which is similar to V_E but spin-dependent, and two intermediate-range (IR) terms $\sim X_{ik}(\mathbf{r}_{ij})\delta(\mathbf{r}_{kj}) + X_{ik}(\mathbf{r}_{kj})\delta(\mathbf{r}_{ij})$ similar to V_D. Note that although the spin-isospin structure is similar to the Urbana IX force and in general to the two-pion-exchange part of the Illinois forces, the spatial functions are quite different. Finally, the coordinate-space expression for the c_4 part of V_C is given in Appendix A. This does not contribute in neutron matter for general regulators due to the isospin structure.

For a many-body system, the total 3N interactions are then given by $V_{3N} = \sum_{i<j<k} V_{3N}^{ijk}$, with $i, j, k = 1, \ldots, A$. Moreover, in the AFDMC calculation V_{3N}^{ijk} is rewritten as a sum over cyclic permutations only.

In order to regularize the local 3N forces consistently with the NN forces of Refs. [23, 24], we replace the δ functions by smeared-out delta functions of the form

$$\delta(\mathbf{r}) \;\to\; \delta_{R_{3N}}(\mathbf{r}) = \frac{1}{\pi \Gamma\big(3/4\big) R_{3N}^3} e^{-(r/R_{3N})^4} , \quad (9)$$

where R_{3N} is the three-body cutoff. For the long-range pion-exchange contributions, we multiply the Yukawa functions with the long-range regulator $f_{\rm long}$ of Refs. [23, 24], given by

$$Y(r) \;\to\; Y(r)\Big(1 - e^{-(r/R_{3N})^4}\Big) . \quad (10)$$

To be consistent with the NN cutoff $R_0 = 1.0 - 1.2\,$fm, we will also vary the 3N cutoff in this range, $R_{3N} = 1.0 - 1.2\,$fm. We have checked that the IR and SR parts of V_C as well as the V_E and V_D contributions in neutron matter vanish for $R_{3N} \to 0$ (for infinite momentum cutoffs), and are therefore regulator effects.

In the following, we include all terms of V_C (the c_1 and c_3 parts for neutron matter), with the c_i couplings given by the NN interactions used [23, 24]. Results including the shorter-range contributions V_D and V_E, which require fits of c_D and c_E, will be studied in Ref. [32].

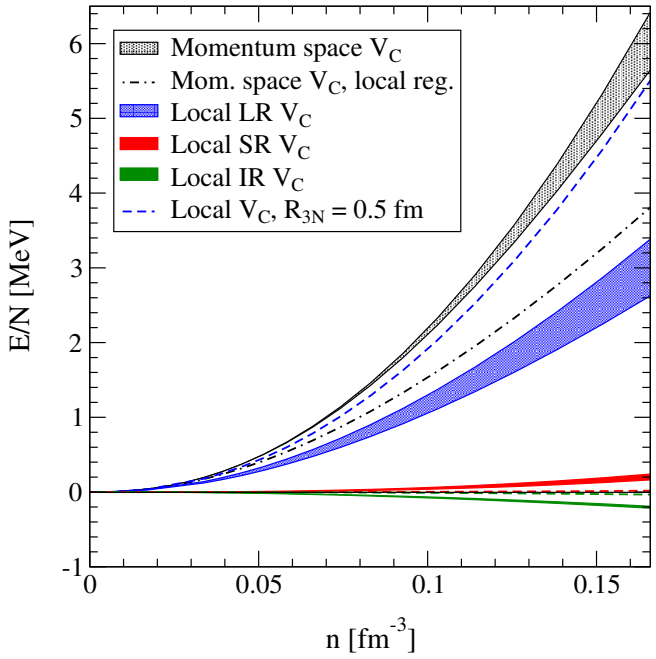

FIG. 2. (Color online) Contributions to the neutron-matter energy per particle E/N as a function of density n at the Hartree-Fock level. The black band shows the energy obtained using a nonlocal regulator, as in Ref. [34], with a 3N cutoff $400 - 500\,$MeV. The blue band corresponds to the LR part of the two-pion-exchange interaction V_C with the local regulator used here, the red band to the SR part of V_C, and the green band to the IR of V_C. For these bands, the cutoff in the local regulator is varied with $R_{3N} = 1.0 - 1.2\,$fm. The dashed-dotted line corresponds to the results for V_C using the local momentum-space regulator of Ref. [31] with a cutoff $\Lambda_{3N} = 500\,$MeV. This shows that these local 3N forces provide less repulsion at the Hartree-Fock level than with nonlocal regulators. The dashed lines show the results for V_C with the local regulator and small $R_{3N} = 0.5\,$fm.

III. HARTREE-FOCK CALCULATION FOR NEUTRON MATTER

We calculate the 3N contributions from the V_C part to neutron matter first at the Hartree-Fock (HF) level. This includes all interactions of Eqs. (7) and (8). Details on the HF calculation can be found in Refs. [34].

In Fig. 2 we show the contributions to the neutron-matter energy per particle E/N as a function of density n. The blue band corresponds to the LR part of the two-pion-exchange interaction V_C with the local regulator used here, the red band to the SR part of V_C, and the green band to the IR of V_C. For these bands, the cutoff in the local regulator is varied between $R_{3N} = 1.0 - 1.2\,$fm. The dashed lines show the results for V_C with the local regulator and $R_{3N} = 0.5\,$fm. In addition, the black band shows the energy obtained using a nonlocal regulator, as in Ref. [34], with a cutoff $400 - 500\,$MeV.

The HF energy in neutron matter for the local V_C are in total $\approx 3\,$MeV at saturation density $n_0 = 0.16\,\text{fm}^{-3}$.

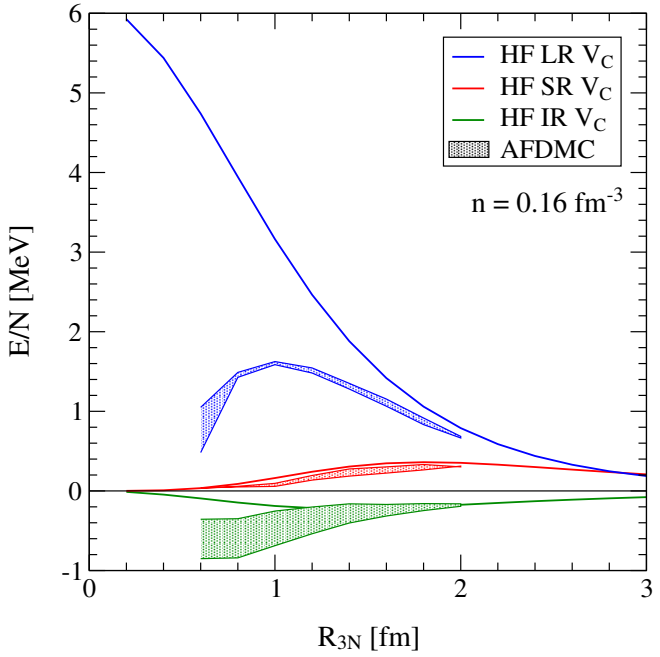

FIG. 3. (Color online) Contributions to the energy per particle E/N at saturation density as a function of the cutoff R_{3N}. The lines show the LR, SR, and IR parts of the two-pion-exchange interaction V_C with the local regulator used here, calculated at the Hartree-Fock level. The bands are the contributions of the corresponding 3N parts to the AFDMC energies for a variation of the NN cutoff $R_0 = 1.0 - 1.2\,\text{fm}$, see also Fig. 4.

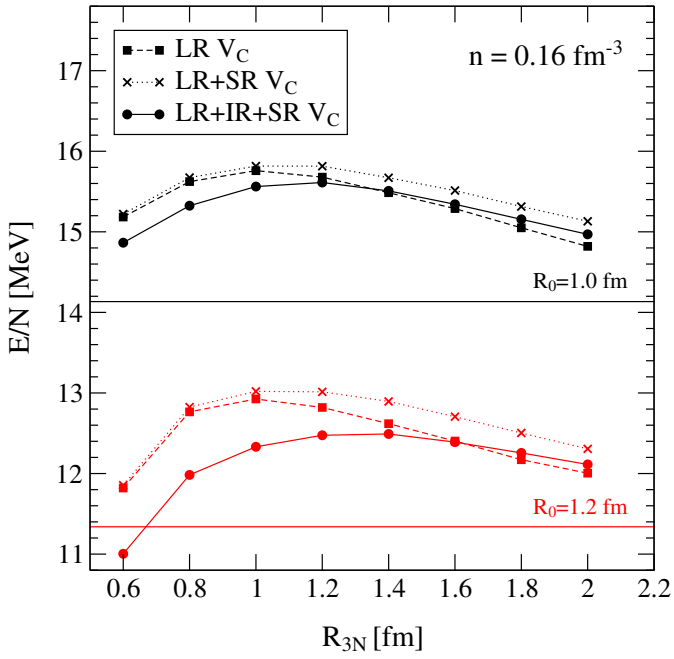

FIG. 4. (Color online) Variation of the AFDMC energy per particle at saturation density as a function of the 3N cutoff R_{3N} for an NN cutoff 1.0 fm (black lines in the upper part) and 1.2 fm (red lines in the lower part). The horizontal lines correspond to the NN-only energy. The squares are for the c_1 and LR c_3 part of V_C, the crosses include also the SR c_3 part of V_C, and the circles include all parts of V_C.

This is only about half of the V_C contribution using the nonlocal regulator. The shorter-range (IR and SR) contributions, which are regulator effects, are small and with opposite sign. If we lower the coordinate-space cutoff, $R_{3N} = 0.5\,\text{fm}$ (dashed lines), we find that the IR and SR parts almost vanish, as expected, and that the total HF energy is 5.5 MeV for the local V_C, which agrees well with the momentum-space result. We also note that the momentum-space result is very close to the infinite-cutoff result at the HF level. Thus, the smaller 3N energies for the local 3N forces are due to the local regulators used.

To check this, we have performed a HF calculation of V_C using the local momentum-space regulator of Ref. [31] with a cutoff of $\Lambda_{3N} = 500\,\text{MeV}$. This is given by the dashed-dotted line in Fig. 2. At saturation density, we find an energy per particle of 3.8 MeV, which is comparable to the result for the local 3N forces used here. This supports the above conclusion that 3N forces with local regulators provide less repulsion at the HF level compared to the usual nonlocal regulators. It may be possible that the V_D and V_E parts, which contribute to neutron matter for local regulators, make up part of these differences. This will be explored further in Ref. [32].

We show the V_C contributions to the energy per particle E/N at saturation density as a function of the 3N cutoff R_{3N} in Fig. 3. The lines show the LR, SR, and IR parts for the local regulator used here, calculated at the HF level. For all 3N cutoffs, the SR and IR parts are small and of opposite sign, while the major contribution of V_C comes from the LR parts. The SR and IR parts vanish for small coordinate-space (high momentum-space) cutoffs, as expected. The LR part increases up to the infinite-cutoff result at the HF level. In the cutoff range $R_{3N} = 1.0 - 1.2\,\text{fm}$, the total contribution of V_C is $\approx 3\,\text{MeV}$, and thus only about half of infinite-cutoff result. This is what we also found in Fig. 2. We emphasize that the cutoff dependence from $400 - 500\,\text{MeV}$ to infinte momentum-space cutoff is small for nonlocal regulators and these densities.

IV. QMC CALCULATION FOR NEUTRON MATTER

Next, we investigate 3N forces in neutron matter using the AFDMC method, similarly to Refs. [23, 24]. In Fig. 3, in addition to the HF results, we show the contributions of the LR, SR, and IR parts of V_C to the AFDMC energy, where the bands are from varying the NN cutoff $R_0 = 1.0 - 1.2\,\text{fm}$. For the SR part, the AFDMC energies agree well with the HF energies, so that HF is a good approximation for this contribution. For the IR part, for large coordinate-space cutoffs, the agreement between HF and AFDMC results is good but worsens for

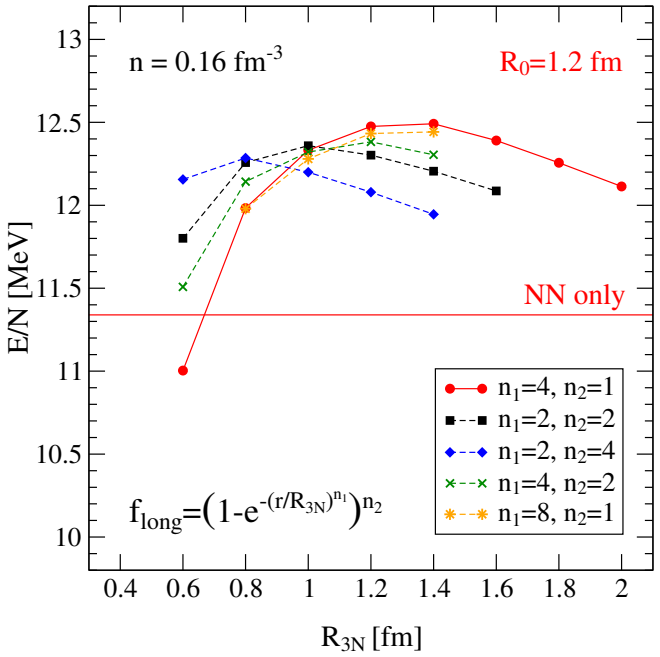

FIG. 5. (Color online) Dependence of the AFDMC energy per particle at saturation density as a function of the 3N cutoff R_{3N} on different long-range regulators. Results are shown for an NN cutoff $R_0 = 1.2\,\text{fm}$. The long-range regulator is given by $\left[1 - e^{-(r/R_{3N})^{n_1}}\right]^{n_2}$ with different parameters n_1 and n_2.

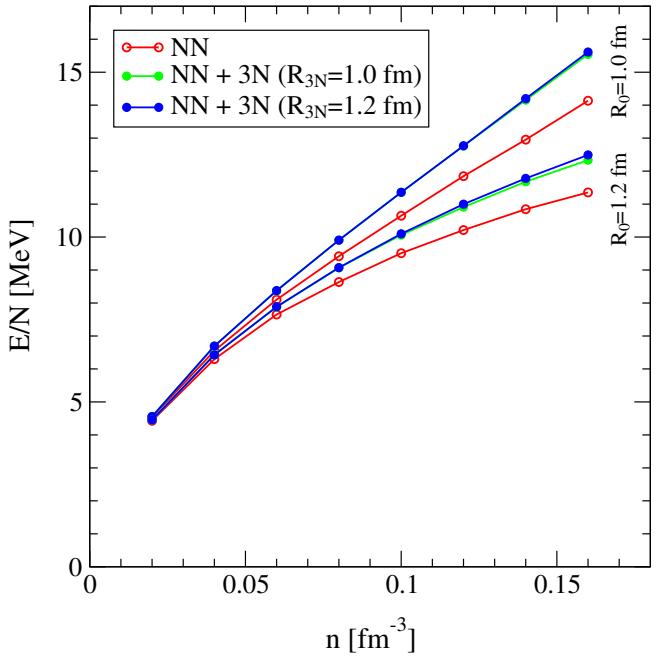

FIG. 6. (Color online) Energy per particle as a function of density for neutron matter at N^{2}LO, including NN forces and the 3N V_C interaction in AFDMC. Results are shown for an NN cutoff $R_0 = 1.0 - 1.2\,\text{fm}$ and R_{3N} in the same range.

smaller cutoffs. The uncertainty (from NN cutoff variation) grows and the energy decreases significantly compared to the HF result. For the LR parts, the AFDMC energies are about $70-80\%$ of the HF energies for higher cutoffs, which suggests that the LR N^{2}LO 3N contributions beyond HF are important. When lowering the 3N cutoff, the energy increases up to a plateau. Further lowering the cutoff, the system collapses and the energy rapidly decreases. In addition, the uncertainty grows.

To study these effects more clearly, we show the variation of the total AFDMC energy per particle at saturation density as a function of the 3N cutoff R_{3N} for an NN cutoff 1.0 fm (black lines in the upper part) and 1.2 fm (red lines in the lower part) in Fig. 4. The horizontal lines correspond to the NN-only energies. The squares include only the LR c_1 and c_3 part of V_C, the crosses include also the SR c_3 part of V_C, and the circles include all parts of V_C. For the soft NN potential ($R_0 = 1.2\,\text{fm}$), we find the plateau of the AFDMC energy to be at $R_{3N} = 1.2 - 1.4\,\text{fm}$. If the cutoff is lowered, the energy decreases and for $R_{3N} = 0.6\,\text{fm}$ we find an attractive 3N contribution.[1] For the harder NN potential ($R_0 = 1.0\,\text{fm}$), the plateau is found for smaller 3N cutoffs, $R_{3N} = 1.0 - 1.2\,\text{fm}$.

[1] This behavior is qualitatively similar to the overbinding given by the Illinois 3N forces in pure neutron systems [35]. It would be interesting to see if using a similar cutoff would avoid the overbinding of neutron matter using Illinois forces.

In general, the plateau is reached when $R_{3N} \sim R_0$, and the system collapses when R_{3N} is significantly smaller than R_0. This can be understood because harder NN potentials do not favor particles to be close and smaller 3N cutoffs are needed to overcome this repulsion. If we want to decrease R_{3N} in our calculations, we also need to decrease R_0. Therefore, R_{3N} has to be chosen consistently with R_0 which justifies our cutoff range. Because $R_0 < 1.0\,\text{fm}$ is difficult for local NN potentials [24], we also do not decrease the 3N cutoff below that limit and use the range for R_0 and R_{3N} within $1.0 - 1.2\,\text{fm}$.

Although the collapse of the system for lower 3N cutoffs does not appear in the HF calculation, it is not an artifact of the AFDMC method. It is due to the function $X_{ij}(\mathbf{r})$, which includes terms $\sim 1/r^3$. If three particles are in a small volume, this becomes very attractive, unless it gets regularized with a large enough R_{3N}. These cutoff values correspond to the position of the plateau. In a HF calculation, which only includes low-momentum states, this collapse will not appear.

We have investigated the AFDMC energies when choosing different parameters in the long-range regulator function. In Fig. 5 we show the dependence of the AFDMC energy per particle at saturation density as a function of the 3N cutoff R_{3N} on different long-range regulators. Results are shown for an NN cutoff $R_0 = 1.2\,\text{fm}$. The long-range regulator is given by $\left(1 - e^{-(r/R_{3N})^{n_1}}\right)^{n_2}$ with different parameters n_1 and n_2. We find that the general picture is independent of the choice of the exponents in the regulator function. A consistent change of

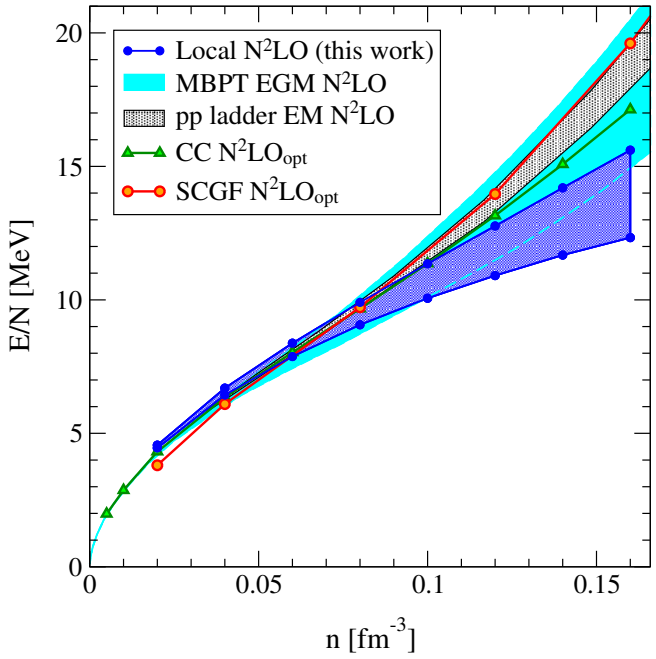

FIG. 7. (Color online) Comparison of the neutron-matter energy at N^{2}LO based on the local chiral NN+3N potentials in AFDMC (this work) with the N^{2}LO calculation of Ref. [10] based on the EGM N^{2}LO potentials and using many-body perturbation theory (MBPT), with the particle-particle (pp) ladder results of Ref. [14] based on the EM N^{2}LO potential, and with results based on the N^{2}LO$_{\rm opt}$ potential using coupled-cluster (CC) theory [11] and self-consistent Green's function (SCGF) methods [13].

the short-range regulator has only a negligible effect on the energy. For different functions, the position of the plateau varies between $0.8-1.2$ fm but the overall energies at the plateau are comparable, generally ranging between $12.3-12.5$ MeV.

In Fig. 6 we present the final result of our AFDMC simulations for the equation of state of neutron matter at N^{2}LO. We show the energy per particle as a function of density including NN forces and the 3N V_C interaction. Results are shown for an NN cutoff $R_0 = 1.0-1.2$ fm and R_{3N} in the same range. For the softer NN potential ($R_0 = 1.2$ fm, lower lines) we find the energy per particle to be $12.3-12.5$ MeV at saturation density for different 3N cutoffs. The NN-only energy is 11.4 MeV and the 3N V_C has an impact of ≈ 1 MeV. For the harder NN potential ($R_0 = 1.0$ fm, upper lines) we find an energy per particle of $15.5-15.6$ MeV compared to 14.1 MeV for an NN-only calculation. Here, the impact of the 3N V_C is ≈ 1.5 MeV. The variation of the total energy with the 3N cutoff is ≈ 0.2 MeV in our cutoff range and considerably smaller than the variation with the NN cutoff, because R_{3N} range lies in the plateau described above.

We find the magnitude of the local 3N two-pion-exchange V_C forces to be at most about 1.5 MeV at saturation density, which is is smaller than a typical contribution of 4 MeV [6] in momentum space with nonlocal regulators, including 2nd and 3rd order corrections. As discussed above, this difference can already be seen on the HF level and is most likely due to the present local regulators. This was also observed in the coupled-cluster calculations of Ref. [11] where a difference of 2 MeV was found for the neutron-matter energy per particle when choosing local versus nonlocal regulators with a similar cutoff of 500 MeV. Following these findings, local versus nonlocal regulators need to be further investigated.

In Fig. 7 we compare the neutron-matter energy at N^{2}LO based on the local chiral NN+3N potentials in AFDMC (this work) with the N^{2}LO calculation of Ref. [10] based on the EGM N^{2}LO potentials of Ref. [36] and using many-body perturbation theory (MBPT), with the particle-particle (pp) ladder results of Ref. [14] based on the EM N^{2}LO potential of Ref. [37], and with results based on the N^{2}LO$_{\rm opt}$ potential of Ref. [38] using self-consistent Green's function (SCGF) methods [13] and using coupled-cluster (CC) theory [11]. At saturation density, the AFDMC energies are in general smaller than the other results, mainly due to the smaller contributions from local 3N forces. Furthermore, the density dependence of the AFDMC band is flatter than for the other calculations, which may be explained by differences in the NN phase shift predictions. We would expect the results to come closer when including chiral forces at next-to-next-to-next-to-leading order (N^{3}LO). A comparison of AFDMC results with MBPT results using the same local potential, as in Refs. [23, 24], will be presented in a forthcoming paper.

V. NEUTRON DROPS

Neutron drops in external potentials provide useful constraints for energy-density functionals and their applications to neutron-rich nuclei [22, 39]. They constitute a simplified model of neutron-rich nuclei, where the external well simulates the effects of the core on the valence neutrons. Their study is therefore a natural addition to homogenous neutron matter.

We have performed AFDMC calculations for the energies and radii of neutron drops with $N = 8$, 20, 40, and 70 neutrons in a harmonic oscillator potential with an oscillator parameter $\hbar\omega = 10$ MeV. For these calculations we used the same cutoff in the NN and 3N interactions, $R_0 = R_{3N} = 1.0-1.2$ fm. The results for the energies and radii are tabulated in Tab. I and shown in Fig. 8. We give the results at different orders in the chiral expansion, and at N^{2}LO, for NN forces only, plus only the LR c_1 and c_3 parts of V_C, and including also the SR and IR parts of V_C. The bands in Fig. 8 are given by the cutoff variation $R_0 = R_{3N} = 1.0-1.2$ fm. We generally find a good order-by-order convergence of the energies and radii. The band increases with neutron numbers, at the level of N^{2}LO+V_C it is 1% for the energy of $N = 8$ neutron drops, 2% for $N = 20$, 5% for $N = 40$, and 7% for $N = 70$. Furthermore, in systems with $N > 20$ and

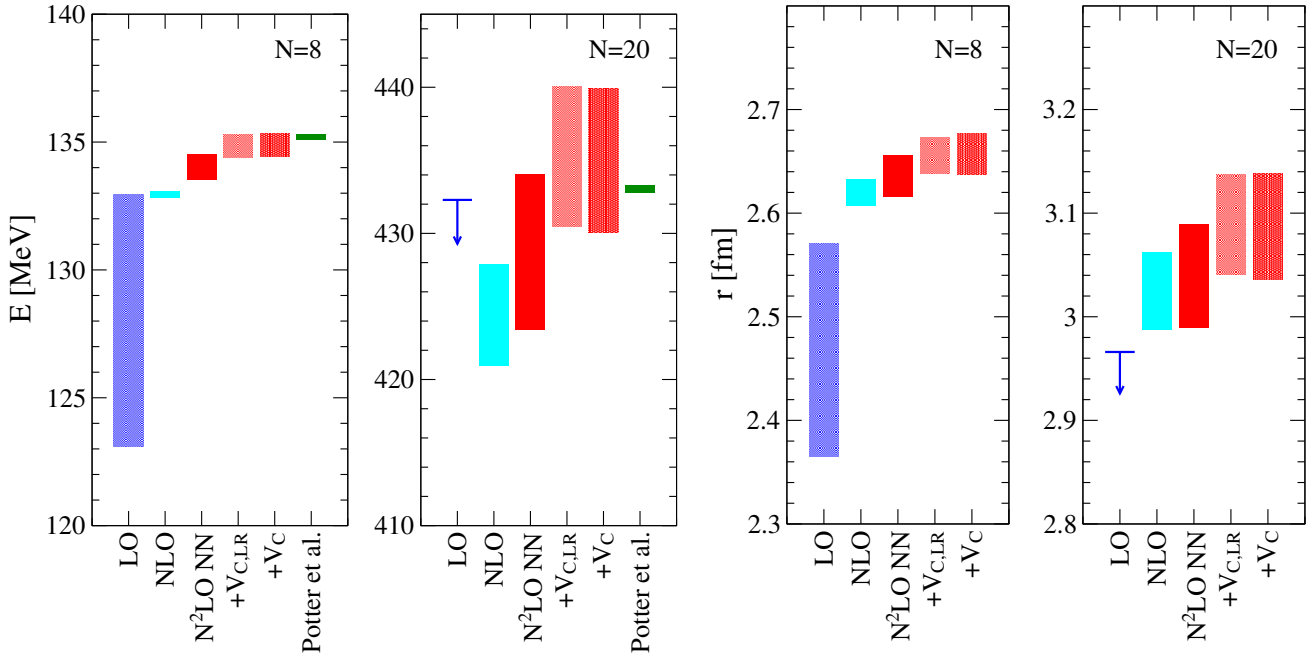

FIG. 8. Energies and radii of neutron drops with $N = 8$ and 20 neutrons in a harmonic oscillator potential with an oscillator parameter $\hbar\omega = 10\,\mathrm{MeV}$ using AFDMC. The same cutoff is used in the NN and 3N interactions. We give the results at different orders in the chiral expansion, and at N^{2}LO, for NN forces only, plus only the LR c_1 and c_3 parts of V_C, and including also the SR and IR parts of V_C. The bands are given by the cutoff variation $R_0 = R_{3N} = 1.0 - 1.2\,\mathrm{fm}$. At LO with the softer cutoff and $N = 20$, the system collapses. We compare our results with the calculations of Ref. [40], using coupled-cluster theory at the ΛCCSD level, where the band is given by two different SRG evolution scales (for one initial NN+3N Hamiltonian).

at low orders, our calculations do not converge and a collapse occurs (for the interactions not listed in the table). This is due to the higher densities inside the larger neutron drops which are also tabulated for the N^{2}LO+V_C Hamiltonian at $r = 0.125$ fm in Table I. These show that the different particle numbers probe a broad range of central densities from low densities for $N = 8$ to twice nuclear saturation density for $N = 70$, connecting the neutron drop results with our neutron matter calculations. The higher the (central) density, the larger the effect of the 3N forces, leading to a collapse for high densities.

Furthermore, for all N at N^{2}LO the relative contribution of V_C is always larger for the $R_0 = 1.2$ fm potential than for the 1.0 fm one. For $N = 70$ we find V_C to contribute 3.7% for 1.2 fm versus 2.7% for 1.0 fm and for $N = 8$ 0.69% versus 0.60%. This result is the opposite of what Fig. 6 shows for homogeneous matter: there the softer NN potential leads to a smaller 3N contribution. This is due to the higher central densities of the neutron drops for the softer potentials, leading to larger 3N contributions.

In Fig. 8, we also compare our results at N^{2}LO with the calculations of Ref. [40] using coupled-cluster theory at the ΛCCSD level. The latter results are based on an SRG-evolved chiral Hamiltonian starting from the N^{3}LO NN potential of Ref. [41] with a cutoff of 500 MeV and local N^{2}LO 3N forces, regulated in momentum space with the same cutoff value, including also the V_D and V_E parts. The band is given by two different SRG evolution scales (for this initial NN+3N Hamiltonian). We find very good agreement between the two approaches after inclusion of N^{2}LO 3N forces, whose contribution is small.

VI. SUMMARY AND OUTLOOK

We have presented local chiral 3N forces at N^{2}LO that are consistent with the local NN interactions of Refs. [23, 24]. We have investigated the 3N two-pion-exchange contributions to neutron matter both at the HF level and in AFDMC calculations, including a detailed study of the regulator dependence. Our results show that present local regulators lead to less repulsion from 3N forces compared to using the usual nonlocal regulators. This is already present at the HF level.

In neutron matter, the dependence on the 3N cutoff over the range $R_{3N} = 1.0 - 1.2\,\mathrm{fm}$ is small compared to the NN cutoff variation, but for lower 3N cutoffs the system starts to collapse. We have also studied the influence of different local 3N regulators and found that the general picture remains the same. Our findings lead to the conclusion that local versus nonlocal regulators have to be extensively studied. It will be crucial to develop a method of assessing the quality of local regulators to find improved versions for these regulators.

TABLE I. Energies (in MeV) and radii (in fm) of neutron drops with $N = 8$, 20, 40, and 70 neutrons in a harmonic oscillator potential with an oscillator parameter $\hbar\omega = 10\,\mathrm{MeV}$. The same cutoff is used in the NN and 3N interactions. We give the results at different orders in the chiral expansion, and at N^{2}LO, for NN forces only, plus only the LR c_1 and c_3 parts of V_C, and including also the SR and IR parts of V_C. For the latter, we also give the central densities (at $r = 0.125$ fm in fm^{-3}). In systems with $N \geqslant 20$ a collapse occurs at low orders (for the interactions not listed in the table).

N	Hamiltonian	E	rms radius	n_c
8	LO(1.0)	132.95(2)	2.571(1)	
8	NLO(1.0)	133.07(3)	2.633(1)	
8	N^{2}LO(1.0) NN-only	134.53(2)	2.656(1)	
8	N^{2}LO(1.0)+$V_{C,\mathrm{LR}}$	135.31(2)	2.673(1)	
8	N^{2}LO(1.0)+V_C	135.34(1)	2.677(1)	0.07(1)
8	LO(1.2)	123.08(5)	2.365(1)	
8	NLO(1.2)	132.82(2)	2.607(1)	
8	N^{2}LO(1.2) NN-only	133.53(1)	2.616(1)	
8	N^{2}LO(1.2)+$V_{C,\mathrm{LR}}$	134.40(1)	2.638(1)	
8	N^{2}LO(1.2)+V_C	134.45(1)	2.637(1)	0.08(1)
20	LO(1.0)	432.29(7)	2.966(1)	
20	NLO(1.0)	427.90(9)	3.062(1)	
20	N^{2}LO(1.0) NN-only	434.04(8)	3.089(1)	
20	N^{2}LO(1.0)+$V_{C,\mathrm{LR}}$	440.04(14)	3.137(1)	
20	N^{2}LO(1.0)+V_C	439.90(7)	3.138(2)	0.15(1)
20	NLO(1.2)	420.92(4)	2.987(1)	
20	N^{2}LO(1.2) NN-only	423.38(3)	2.989(1)	
20	N^{2}LO(1.2)+$V_{C,\mathrm{LR}}$	430.45(6)	3.041(1)	
20	N^{2}LO(1.2)+V_C	430.05(5)	3.036(1)	0.18(1)
40	NLO(1.0)	1053.10(36)	3.459(1)	
40	N^{2}LO(1.0) NN-only	1068.31(13)	3.481(1)	
40	N^{2}LO(1.0)+$V_{C,\mathrm{LR}}$	1091.97(23)	3.557(1)	
40	N^{2}LO(1.0)+V_C	1090.28(14)	3.556(1)	0.16(1)
40	NLO(1.2)	1015.09(15)	3.318(1)	
40	N^{2}LO(1.2) NN-only	1015.35(17)	3.293(1)	
40	N^{2}LO(1.2)+$V_{C,\mathrm{LR}}$	1045.77(12)	3.385(1)	
40	N^{2}LO(1.2)+V_C	1042.31(16)	3.377(1)	0.20(1)
70	N^{2}LO(1.0) NN-only	2230.26(26)	3.877(1)	
70	N^{2}LO(1.0)+$V_{C,\mathrm{LR}}$	2296.42(64)	3.987(1)	
70	N^{2}LO(1.0)+V_C	2290.60(25)	3.991(1)	0.25(2)
70	N^{2}LO(1.2) NN-only	2062.93(59)	3.593(1)	
70	N^{2}LO(1.2)+$V_{C,\mathrm{LR}}$	2155.56(48)	3.730(2)	
70	N^{2}LO(1.2)+V_C	2139.78(54)	3.711(2)	0.31(2)

We have studied the neutron-matter equation of state for local chiral NN and 3N interactions and found smaller energies compared to other calculations, mainly due to less repulsion from 3N forces. We also simulated neutron drops in an external harmonic oscillator potential for neutron number $N = 8$, 20, 40 and 70 and investigated their energies and radii for different chiral orders. Our results show a very good agreement with previous coupled-cluster calculations using chiral potentials [40] (also with local 3N forces).

Work on the determination of the two 3N couplings c_D and c_E for the local 3N forces is in preparation [32]. The inclusion of the full N^{2}LO 3N forces will enable novel many-body calculations of nuclei and nuclear matter with QMC methods based on chiral EFT interactions.

ACKNOWLEDGMENTS

We thank J. Carlson, R. Furnstahl, K. Hebeler, J. Lynn, A. Lovato, and K. Schmidt for useful discussions. This work was supported in part by the ERC Grant No. 307986 STRONGINT, the Natural Sciences and Engineering Research Council of Canada, the US Department of Energy, Office of Nuclear Physics, under Contract DE-AC02-05CH11231, the NUCLEI SciDAC program, and the LANL LDRD program. The computations were performed at the Jülich Supercomputing Center. We also used resources provided by Los Alamos Open Supercomputing and by NERSC, which is supported by the US Department of Energy, Office of Science, under Contract DE-AC02-05CH11231.

Appendix A: Coordinate-space expressions

In momentum space, the N^{2}LO 3N interactions are given by [4, 5]

$$V_C = \frac{1}{2}\left(\frac{g_A}{2f_\pi}\right)^2 \sum_{\pi(ijk)} \frac{\boldsymbol{\sigma}_i\cdot\mathbf{q}_i\,\boldsymbol{\sigma}_k\cdot\mathbf{q}_k}{(q_i^2+m_\pi^2)(q_k^2+m_\pi^2)}\, F_{ijk}^{\alpha\beta}\,\tau_i^\alpha\,\tau_k^\beta\,, \tag{A1}$$

$$V_D = -\frac{g_A}{8f_\pi^2}\frac{c_D}{f_\pi^2\Lambda_\chi}\sum_{\pi(ijk)}\frac{\boldsymbol{\sigma}_k\cdot\mathbf{q}_k}{q_k^2+m_\pi^2}\,\boldsymbol{\sigma}_i\cdot\mathbf{q}_k\,\boldsymbol{\tau}_i\cdot\boldsymbol{\tau}_k\,, \tag{A2}$$

$$V_E = \frac{c_E}{2f_\pi^4\Lambda_\chi}\sum_{\pi(ijk)}\boldsymbol{\tau}_i\cdot\boldsymbol{\tau}_k\,, \tag{A3}$$

where $\mathbf{q}_i = \mathbf{p}_i' - \mathbf{p}_i$ is the momentum transfer of particle i (all other quantities are defined in Sec. II) and $F_{ijk}^{\alpha\beta}$ includes the different contributions from the c_i's

$$F_{ijk}^{\alpha\beta} = \delta^{\alpha\beta}\left[-\frac{4c_1m_\pi^2}{f_\pi^2}+\frac{2c_3}{f_\pi^2}\,\mathbf{q}_i\cdot\mathbf{q}_k\right] + \sum_\gamma\frac{c_4}{f_\pi^2}\varepsilon^{\alpha\beta\gamma}\,\tau_j^\gamma\,\boldsymbol{\sigma}_j\cdot(\mathbf{q}_i\times\mathbf{q}_k)\,. \tag{A4}$$

In neutron matter, the 3N contributions simplify because the isospin structure can be evaluated explicitly, with all $\boldsymbol{\tau}_i\cdot\boldsymbol{\tau}_j = 1$ and the c_4 part vanishes [6].

We Fourier transform the 3N interactions with respect to the momentum transfers of particle i and k, which yields the coordinate-space expression V^{ijk} as a function of $\mathbf{r}_{ij}$ and $\mathbf{r}_{kj}$. Because the 3N interactions include a

sum over all permutations, taking a different choice for the momentum transfers would lead to the same result. However, this will not be the case when a regulator in momentum space is included before Fourier transforming. For the V_E contribution this gives

$$V_E^{ijk} = \int \frac{d^3q_i}{(2\pi)^3}\frac{d^3q_k}{(2\pi)^3}\, e^{i\mathbf{q}_i\cdot\mathbf{r}_{ij}}\, e^{i\mathbf{q}_k\cdot\mathbf{r}_{kj}}\, V_E\,, \\ = \frac{c_E}{2f_\pi^4\Lambda_\chi}\sum_{\pi(ijk)} \boldsymbol{\tau}_i\cdot\boldsymbol{\tau}_k\,\delta(\mathbf{r}_{ij})\delta(\mathbf{r}_{kj})\,. \tag{A5}$$

For the Fourier transformation of the V_D contribution one has

$$V_D^{ijk} = \int \frac{d^3q_i}{(2\pi)^3}\frac{d^3q_k}{(2\pi)^3}\, e^{i\mathbf{q}_i\cdot\mathbf{r}_{ij}}\, e^{i\mathbf{q}_k\cdot\mathbf{r}_{kj}}\, V_D\,, \\ = -\frac{c_D g_A}{8f_\pi^4\Lambda_\chi}\sum_{\pi(ijk)} \boldsymbol{\tau}_i\cdot\boldsymbol{\tau}_k \int \frac{d^3q_i}{(2\pi)^3}\, e^{i\mathbf{q}_i\cdot\mathbf{r}_{ij}} \\ \times \int \frac{d^3q_k}{(2\pi)^3}\frac{\boldsymbol{\sigma}_k\cdot\mathbf{q}_k\,\boldsymbol{\sigma}_i\cdot\mathbf{q}_k}{q_k^2+m_\pi^2}\, e^{i\mathbf{q}_k\cdot\mathbf{r}_{kj}}\,. \tag{A6}$$

The second integral gives an expression similar to one-pion exchange:

$$\int \frac{d^3q_k}{(2\pi)^3}\frac{\boldsymbol{\sigma}_k\cdot\mathbf{q}_k\,\boldsymbol{\sigma}_i\cdot\mathbf{q}_k}{q_k^2+m_\pi^2}\, e^{i\mathbf{q}_k\cdot\mathbf{r}_{kj}} \\ = -\frac{m_\pi^2}{12\pi}X_{ik}(\mathbf{r}_{kj}) + \frac{1}{3}\,\boldsymbol{\sigma}_i\cdot\boldsymbol{\sigma}_k\,\delta(\mathbf{r}_{kj})\,, \tag{A7}$$

with $X_{ik}(\mathbf{r})$ defined in Eq. (6). As a result, in addition to the one-pion-exchange–contact part, the Fourier transformation also leads to a contact–contact part in V_D^{ijk}:

$$V_D^{ijk} = \frac{c_D g_A}{24f_\pi^4\Lambda_\chi}\sum_{\pi(ijk)} \boldsymbol{\tau}_i\cdot\boldsymbol{\tau}_k\Big[\frac{m_\pi^2}{4\pi}\,\delta(\mathbf{r}_{ij})X_{ik}(\mathbf{r}_{kj}) \\ - \boldsymbol{\sigma}_i\cdot\boldsymbol{\sigma}_k\,\delta(\mathbf{r}_{ij})\delta(\mathbf{r}_{kj})\Big]\,. \tag{A8}$$

For the c_1 part of V_C we have

$$V_{C,c_1}^{ijk} = -\frac{c_1 m_\pi^2 g_A^2}{2f_\pi^4}\sum_{\pi(ijk)} \boldsymbol{\tau}_i\cdot\boldsymbol{\tau}_k \int \frac{d^3q_i}{(2\pi)^3}\frac{\boldsymbol{\sigma}_i\cdot\mathbf{q}_i}{q_i^2+m_\pi^2}\, e^{i\mathbf{q}_i\cdot\mathbf{r}_{ij}} \\ \times \int \frac{d^3q_k}{(2\pi)^3}\frac{\boldsymbol{\sigma}_k\cdot\mathbf{q}_k}{q_k^2+m_\pi^2}\, e^{i\mathbf{q}_k\cdot\mathbf{r}_{kj}}\,. \tag{A9}$$

The integrals are readily evaluated using

$$\int \frac{d^3q_i}{(2\pi)^3}\frac{\boldsymbol{\sigma}_i\cdot\mathbf{q}_i}{q_i^2+m_\pi^2}\, e^{i\mathbf{q}_i\cdot\mathbf{r}_{ij}} \\ = -\,i\,\sigma_i^\alpha\,\partial^\alpha\,\frac{e^{-m_\pi r_{ij}}}{4\pi r_{ij}} = i\,\frac{m_\pi}{4\pi}\,\sigma_i^\alpha\,\hat r_{ij}^\alpha\,U(r_{ij})Y(r_{ij})\,. \tag{A10}$$

This leads to

$$V_{C,c_1}^{ijk} = \frac{c_1 m_\pi^4 g_A^2}{2f_\pi^4(4\pi)^2}\sum_{\pi(ijk)} \boldsymbol{\tau}_i\cdot\boldsymbol{\tau}_k\,\boldsymbol{\sigma}_i\cdot\hat{\mathbf{r}}_{ij}\,\boldsymbol{\sigma}_k\cdot\hat{\mathbf{r}}_{kj} \\ \times U(r_{ij})Y(r_{ij})U(r_{kj})Y(r_{kj})\,. \tag{A11}$$

Next, the Fourier transformation of the c_3 part of V_C gives

$$V_{C,c_3}^{ijk} = \frac{c_3 g_A^2}{4f_\pi^4}\sum_{\pi(ijk)} \boldsymbol{\tau}_i\cdot\boldsymbol{\tau}_k \int \frac{d^3q_i}{(2\pi)^3}\frac{\boldsymbol{\sigma}_i\cdot\mathbf{q}_i}{q_i^2+m_\pi^2}\, q_i^\alpha\, e^{i\mathbf{q}_i\cdot\mathbf{r}_{ij}} \\ \times \int \frac{d^3q_k}{(2\pi)^3}\frac{\boldsymbol{\sigma}_k\cdot\mathbf{q}_k}{q_k^2+m_\pi^2}\, q_k^\alpha\, e^{i\mathbf{q}_k\cdot\mathbf{r}_{kj}}\,. \tag{A12}$$

Similar to the Fourier transformation for one-pion exchange in Eq. (A7) one gets

$$\int \frac{d^3q_i}{(2\pi)^3}\frac{\boldsymbol{\sigma}_i\cdot\mathbf{q}_i}{q_i^2+m_\pi^2}\, q_i^\alpha\, e^{i\mathbf{q}_i\cdot\mathbf{r}_{ij}} \\ = -\frac{m_\pi^2}{4\pi}\,\sigma_i^\beta\Big[\Big(\hat r_{ij}^\alpha\,\hat r_{ij}^\beta - \frac{1}{3}\,\delta^{\alpha\beta}\Big)\,T(r_{ij})Y(r_{ij}) \\ + \frac{1}{3}\,\delta^{\alpha\beta}\,Y(r_{ij}) - \frac{1}{3}\frac{4\pi}{m_\pi^2}\,\delta^{\alpha\beta}\,\delta(\mathbf{r}_{ij})\Big]\,. \tag{A13}$$

Combining this leads to

$$V_{C,c_3}^{ijk} = \frac{c_3 g_A^2}{36f_\pi^4}\sum_{\pi(ijk)} \boldsymbol{\tau}_i\cdot\boldsymbol{\tau}_k \\ \times\Big[\frac{m_\pi^4}{(4\pi)^2}\,X_{ij}(\mathbf{r}_{ij})X_{kj}(\mathbf{r}_{kj}) - \frac{m_\pi^2}{4\pi}\,X_{ik}(\mathbf{r}_{ij})\delta(\mathbf{r}_{kj}) \\ - \frac{m_\pi^2}{4\pi}\,X_{ik}(\mathbf{r}_{kj})\delta(\mathbf{r}_{ij}) + \boldsymbol{\sigma}_i\cdot\boldsymbol{\sigma}_k\delta(\mathbf{r}_{ij})\,\delta(\mathbf{r}_{kj})\Big]\,. \tag{A14}$$

Finally, for the c_4 part of V_C we obtain

$$V_{C,c_4}^{ijk} = \frac{c_4 g_A^2}{72f_\pi^4}\sum_{\pi(ijk)} \boldsymbol{\tau}_i\cdot(\boldsymbol{\tau}_k\times\boldsymbol{\tau}_j) \\ \times\Big[\frac{m_\pi^4}{2i(4\pi)^2}[X_{ij}(\mathbf{r}_{ij}),X_{kj}(\mathbf{r}_{kj})] \\ - \frac{m_\pi^2}{4\pi}\boldsymbol{\sigma}_i\cdot(\boldsymbol{\sigma}_k\times\boldsymbol{\sigma}_j)(1-T(r_{ij}))Y(r_{ij})\delta(\mathbf{r}_{kj}) \\ - \frac{m_\pi^2}{4\pi}\boldsymbol{\sigma}_i\cdot(\boldsymbol{\sigma}_k\times\boldsymbol{\sigma}_j)\,(1-T(r_{kj}))\,Y(r_{kj})\delta(\mathbf{r}_{ij}) \\ - \frac{3m_\pi^2}{4\pi}\boldsymbol{\sigma}_i\cdot\hat{\mathbf{r}}_{ij}\,\hat{\mathbf{r}}_{ij}\cdot(\boldsymbol{\sigma}_k\times\boldsymbol{\sigma}_j)T(r_{ij})Y(r_{ij})\delta(\mathbf{r}_{kj}) \\ - \frac{3m_\pi^2}{4\pi}\boldsymbol{\sigma}_k\cdot\hat{\mathbf{r}}_{kj}\,\hat{\mathbf{r}}_{kj}\cdot(\boldsymbol{\sigma}_j\times\boldsymbol{\sigma}_i)T(r_{kj})Y(r_{kj})\delta(\mathbf{r}_{ij}) \\ + \boldsymbol{\sigma}_i\cdot(\boldsymbol{\sigma}_k\times\boldsymbol{\sigma}_j)\delta(\mathbf{r}_{ij})\delta(\mathbf{r}_{kj})\Big]\,. \tag{A15}$$

[1] E. Epelbaum, H.-W. Hammer, and U.-G. Meißner, Rev. Mod. Phys. **81**, 1773 (2009).
[2] R. Machleidt and D. R. Entem, Phys. Rept. **503**, 1 (2011).
[3] H.-W. Hammer, A. Nogga, and A. Schwenk, Rev. Mod. Phys. **85**, 197 (2013).
[4] U. van Kolck, Phys. Rev. C **49**, 2932 (1994).
[5] E. Epelbaum, A. Nogga, W. Glöckle, H. Kamada, U.-G. Meißner, and H. Witała, Phys. Rev. C **66**, 064001 (2002).
[6] K. Hebeler and A. Schwenk, Phys. Rev. C **82**, 014314 (2010).
[7] K. Hebeler, S. K. Bogner, R. J. Furnstahl, A. Nogga, and A. Schwenk, Phys. Rev. C **83**, 031301 (2011).
[8] S. Gandolfi, J. Carlson, and S. Reddy, Phys. Rev. C **85**, 032801 (2012).
[9] J. W. Holt, N. Kaiser, and W. Weise, Prog. Part. Nucl. Phys. **73**, 35 (2013).
[10] I. Tews, T. Krüger, K. Hebeler, and A. Schwenk, Phys. Rev. Lett. **110**, 032504 (2013).
[11] G. Hagen, T. Papenbrock, A. Ekström, K. A. Wendt, G. Baardsen, S. Gandolfi, M. Hjorth-Jensen, and C. J. Horowitz, Phys. Rev. C **89**, 014319 (2014).
[12] C. Wellenhofer, J. W. Holt, N. Kaiser, and W. Weise, Phys. Rev. C **89**, 064009 (2014).
[13] A. Carbone, A. Rios, and A. Polls, Phys. Rev. C **90**, 054322 (2014).
[14] F. Sammarruca, L. Coraggio, J. W. Holt, N. Itaco, R. Machleidt, and L. E. Marcucci, Phys. Rev. C **91**, 054311 (2015).
[15] D. M. Ceperley, Rev. Mod. Phys. **67**, 279 (1995).
[16] J. Carlson, S. Gandolfi, and A. Gezerlis, Prog. Theor. Exp. Phys. (**2012**) 01A209.
[17] B. S. Pudliner, V. R. Pandharipande, J. Carlson, S. C. Pieper, and R. B. Wiringa, Phys. Rev. C **56**, 1720 (1997).
[18] S. C. Pieper, and R. B. Wiringa, Annu. Rev. Nucl. Part. Sci. **51**, 53 (2001).
[19] K. M. Nollett, S. C. Pieper, R. B. Wiringa, J. Carlson, and G. M. Hale, Phys. Rev. Lett. **99**, 022502 (2007).
[20] K. E. Schmidt and S. Fantoni, Phys. Lett. B **446**, 99 (1999).
[21] J. Carlson, S. Gandolfi, F. Pederiva, S. C. Pieper, R. Schiavilla, K. E. Schmidt, and R. B. Wiringa, arXiv:1412.3081.
[22] P. Maris, J. P. Vary, S. Gandolfi, J. Carlson, and S. C. Pieper, Phys. Rev. C **87**, 054318 (2013).
[23] A. Gezerlis, I. Tews, E. Epelbaum, S. Gandolfi, K. Hebeler, A. Nogga, and A. Schwenk, Phys. Rev. Lett. **111**, 032501 (2013).
[24] A. Gezerlis, I. Tews, E. Epelbaum, M. Freunek, S. Gandolfi, K. Hebeler, A. Nogga, and A. Schwenk, Phys. Rev. C **90**, 054323 (2014).
[25] J. E. Lynn, J. Carlson, E. Epelbaum, S. Gandolfi, A. Gezerlis, and A. Schwenk, Phys. Rev. Lett. **113**, 192501 (2014).
[26] M. Piarulli, L. Girlanda, R. Schiavilla, R. Navarro Pérez, J. E. Amaro, and E. Ruiz Arriola, Phys. Rev. C **91**, 024003 (2015).
[27] E. Epelbaum, H. Krebs, D. Lee, and U.-G. Meißner, Eur. Phys. J. A **40**, 199 (2009).
[28] A. Roggero, A. Mukherjee, and F. Pederiva, Phys. Rev. Lett. **112**, 221103 (2014).
[29] G. Wlazłowski, J. W. Holt, S. Moroz, A. Bulgac, and K. J. Roche, Phys. Rev. Lett. **113**, 182503 (2014).
[30] A. Lovato, O. Benhar, S. Fantoni, and K. E. Schmidt, Phys. Rev. C **85**, 024003 (2012).
[31] P. Navrátil, Few Body Syst. **41**, 117 (2007).
[32] J. E. Lynn, J. Carlson, S. Gandolfi, A. Gezerlis, K. E. Schmidt, A. Schwenk, and I. Tews, arXiv:1509.03470.
[33] S. C. Pieper, V. R. Pandharipande, R. B. Wiringa, and J. Carlson, Phys. Rev. C **64**, 014001 (2001).
[34] T. Krüger, I. Tews, K. Hebeler, and A. Schwenk, Phys. Rev. C **88**, 025802 (2013).
[35] A. Sarsa, S. Fantoni, K. E. Schmidt, and F. Pederiva, Phys. Rev. C **68**, 024308 (2003).
[36] E. Epelbaum, W. Glöckle, and U.-G. Meißner, Nucl. Phys. A **747**, 362 (2005).
[37] E. Marji, A. Canul, Q. MacPherson, R. Winzer, Ch. Zeoli, D. R. Entem, and R. Machleidt, Phys. Rev. C **88**, 054002 (2013).
[38] A. Ekström, G. Baardsen, C. Forssen, G. Hagen, M. Hjorth-Jensen, G. R. Jansen, R. Machleidt, W. Nazarewicz, T. Papenbrock, J. Sarich, and S. M. Wild, Phys. Rev. Lett. **110**, 192502 (2013).
[39] S. K. Bogner, R. J. Furnstahl, H. Hergert, M. Kortelainen, P. Maris, M. Stoitsov, and J. P. Vary, Phys. Rev. C **84**, 044306 (2011).
[40] H. D. Potter, S. Fischer, P. Maris, J. P. Vary, S. Binder, A. Calci, J. Langhammer, and R. Roth, Phys. Lett. B **739**, 445 (2015).
[41] D. R. Entem and R. Machleidt, Phys. Rev. C **68**, 041001 (2003).